Indian Journal of Pure & Applied Physics
Vol. 64, August 2026, pp. 842-852
DOI: 10.56042/ijpap.v64i8.30649

Enhanced Energy Harvesting Performance of Flexible PVDF Piezoelectric Nanogenerators using $SnS_2/SnSe_2$ Heterostructure as Nanofillers

Pragya Dobhal, Umesh Kumar, Ankita Dahiya & Bharti Singh*

Department of Applied Physics, Delhi Technological University, Delhi 110 042, India

Received: 10th April 2026; accepted: 18th May 2026

The effect of 2D transition metal dichalcogenides (TMDCs) including SnS_2, $SnSe_2$, their heterostructure ($SnS_2/SnSe_2$) and Polyvinylidene fluoride (PVDF) based composite films for improved performance of piezoelectric nanogenerators (PENG) is reported. SnS_2, $SnSe_2$ and $SnS_2/SnSe_2$ heterostructure were synthesized using hydrothermal method. These TMDC materials were incorporated within a PVDF matrix to create flexible thin films using the solution-casting method in order to investigate their outcome as nanofillers within the PVDF polymer framework. X-ray diffraction (XRD) confirmed the phase purity of SnS_2, $SnSe_2$ and their heterostructure, while the Raman spectra verified vibrational modes indicating high crystallinity and interfacial coupling. The enhancement of piezoelectric behaviour was revealed by Fourier transform infrared spectroscopy (FTIR), which showed an increment in the β-phase of PVDF post adding the TMDC nanofillers. PVDF/SnS_2/$SnSe_2$ heterostructure based nanogenerator exhibited the maximum open circuit voltage (peak-to-peak) (V_{oc}) of 13.2 V and short circuit current (I_{sc}) of 0.87 μA. This improvement is linked to the synergistic effect of the formation of a heterointerface, facilitating charge separation, enhanced stress transfer and polarization due to asymmetric charge distribution at the interface. The generated voltage from the PENG device was used to power an LED. Therefore, our work highlights the application of 2D heterostructure engineering for improving piezoelectric performance and next-generation flexible energy harvesting devices.

Keywords: PVDF polymer, Piezoelectric nanogenerators, Heterostructure nanofillers, 2D $SnS_2/SnSe_2$ heterostructure, Energy harvesting, β- phase enhancement

1. Introduction

The exponentially increasing need of viable and autonomous energy sources has resulted in an advancement in the areas related to self-powered sensors and wearable electronics[1]. There is a necessity for developing alternative energy harvesting technologies as conventional methods suffer from limited life span, environmental concerns and maintenance requirements[2]. This makes piezoelectric nanogenerators (PENGs) highly efficient candidates for enhancing the next generation of flexible and portable devices as they harness electrical energy from mechanical energy on being exposed to stress[3-4].

Polymers like Polyvinylidene fluoride (PVDF) have garnered substantial attention as a piezoelectric material owing to its flexibility, chemical stability, bio-compatibility and ease of fabrication[5]. However, pristine PVDF has a low piezoelectric output adhering to the dominance of the non-polar α-phase[6]. The β-phase being electro-active in nature is responsible for piezoelectric and ferroelectric properties due to the presence of an all Trans (TTTT) conformation[7]. Therefore, the key challenge in improving the performance of PVDF based nanogenerators is the efficient enhancement of the β-phase[8]. To improve the dipole alignment within the polymer matrix and to induce β-phase formation, various strategies like mechanical stretching, electrical-poling and the incorporation of nanofillers[9] have been explored[10].

Out of all the strategies, the incorporation of 2D nanomaterials as fillers has proven to be efficient for the enhancement of the piezoelectric properties of PVDF based nanocomposites[11-12]. These materials have high surface area, efficient stress and charge transfer and strong interfacial interaction[13]. These properties enable effective β-phase nucleation and improved polarization[14]. In this context, the transition metal dichalcogenides (TMDCs) have gained considerable value owing to their layered structure and inherent piezo-electric attributes under broken symmetry conditions[15]. An enhanced piezoelectric output was reported for a chemically exfoliated $MoSe_2$/PVDF nanocomposites, thereby reiterating the role of TMDCs as an effective nanofiller leading to improved polarization and dipole alignment[3].

*Corresponding author: E-mail: bhartisingh@dtu.ac.in

Tin-based dichalcogenides such as SnS_2[16] and $SnSe_2$[17] have shown potential as strong candidates for piezoelectric energy harvesting because of their intrinsic piezoelectric properties as well as strong electro-mechanical coupling[18]. A PVDF/SnS_2 based piezoelectric nanogenerator fabricated using hydrothermal method was reported which led to enhanced, β- phase nucleation and improved electrical outputs[19]. Similarly, more studies on SnS_2 by varying filler concentration have shown that optimized loading enhances piezoelectric performance[20]. Apart from this, advanced nanostructures such as SnS_2 nanoflowers have also highlighted the potential of Tin-based dichalcogenides for efficient energy harvesting[21].

Going beyond single component systems, the engineering of heterostructures has surfaced as a powerful methodology for the enhancement of piezoelectric performance[22]. A heterostructure in 2D materials refers to the stacking of two or more atomically thin layers with different compositions, thus forming a van-der Waals interface without lattice matching constraints[23]. This permits the creation of electromechanical properties via band-alignment and controlled coupling between the layers[24]. In a heterostructure, the number of layers remain uncontrollable and intrinsically non-uniform due to the nucleation of materials and uncontrolled restacking during synthesis. With reference to 2D systems, heterostructure engineering requires careful optimization of parameters like stacking order, twist-angle, phase and composition which controls charge distribution, polarization and electronic structure at the interface[25]. The inbuilt electric field and interfacial dipoles facilitates charge separation and enhanced carrier transport across the interface[26]. These effects along with strain and asymmetry in layered materials lead to improved piezoelectric and optoelectronic performances as compared to their individual counterparts[27].

SnS_2 based heterostructures were also reported which demonstrate improved performance as compared to individual materials due to the creation of an inherent electric field and charge separation at the interface[28-29]. In addition to this, by varying chalcogen atoms (such as S and Se) the electronic structure, dipole distribution and polarization behaviour of TMDCs can be tuned[30]. In spite of these advancements, studies systematically focusing on the effect of chalcogen variation and heterostructure formation in Tin based dichalcogenides enhanced with PVDF still remain unexplored.

Taking this forward, our present work shows a systematic investigation of TMDCs such as SnS_2, $SnSe_2$ and their heterostructure ($SnS_2/SnSe_2$) used as nanofillers in integration with PVDF for piezoelectric nanogenerator applications. The choice of these materials especially SnS_2 and $SnSe_2$ was made due to their intrinsically layered van-der Waals structure[31], tunable electric properties and proven potential in electromechanical energy conversion systems[32]. As per recent studies, it is highlighted theoretically that Se atom in $SnSe_2$ possess a larger ionic radius and lower electronegativity as compared to its S counterpart, thereby exhibiting improved lattice polarizability and dielectric response[33-34]. In addition to this, both SnS_2 and $SnSe_2$ have a complementary band structure and comparable lattice constants, thus enabling the formation of high quality heterointerfaces with minimal lattice mismatch[35]. Structures like these have been shown to induce strong interfacial coupling, charge redistribution and inherent electric field, hence improving carrier separation and functional performance as compared to the individual material.

The selection of a heterostructure configuration in this study is motivated by the limitations fundamentally present in a single-component nanocomposite system. The piezoelectric enhancement which is achieved by the incorporation of an individual 2D nanofiller within the PVDF matrix remains constrained by finite interfacial charge density, limited dipole alignment and inadequate band structure modulation[14]. However, in vertically or laterally stacked 2D heterostructures which are formed between materials with lattice compatibility, such as SnS_2 and $SnSe_2$, exhibit an intrinsic electric field at the interface which arises from the band offset discontinuities and the equilibration of the Fermi level across the heterojunction[36]. This configuration synergistically increases the β-phase nucleation and poling efficiency within the PVDF matrix[37]. Furthermore, the electronegativity gradient introduced by chalcogen substitution improves the interfacial electrostatic environment in a way which cannot be attained by either of the constituent materials individually[38]. All these parameters collectively render heterostructure designing as a grounded strategy for enhancing the performance of conventionally used single-filler PENGs[39].

In this study, X-ray diffraction (XRD) for synthesized powders and films was used for structural analysis. From the results of Fourier transform infrared spectroscopy (FTIR), analysis of the impact

of different 2D nanofillers in PVDF matrix shows substantial enhancement in the electroactive , β- phase of PVDF. Raman spectroscopy was used to detect vibrational modes present in the 2D nanofillers. The Field emission scanning electron microscopy (FESEM) gave detailed findings for the morphological surface structure and uniform dispersion of nanofillers in the composite films. Polarization-Electric field (PE) hysteresis loop was used to evaluate ferroelectric properties and for showing the enhancement in polarization due to β-phase crystallization. The measurements for the values of open circuit voltage (peak-to-peak) (V_{oc}) and short-circuit Current (I_{sc}) were made to analyse the electrical properties of nanogenerators under mechanical stress.

2 Experimental Details

2.1 Materials

Tin (IV) chloride penta-hydrate, Thiourea, Selenium dioxide and PVDF were commercially purchased from Sigma Aldrich. The solvents - Ethylene glycol and N, N-dimethyl formamide (DMF) were procured from Thermo Fisher and were utilized as received.

2.2 Synthesis of SnS_2 Powder

Tin (II) Sulphide was synthesized in its powder form using hydrothermal method. Tin (IV) chloride penta-hydrate (3 mmol) and Thiourea (5 mmol) were used as the precursor reagents and were blended in 40 mL of de-ionized water. The solution was magnetically stirred for 45 minutes at room temperature. It was further put into a Teflon container and sealed into a stainless-steel autoclave. It was then heated in the hot air oven at 200 °C for 24 hours. Post this, the sample was washed twice with de-ionized water and ethanol and centrifuged for 6 minutes at 5500 rpm. It was then left to dry in a vacuum oven overnight at 80 °C. Yellowish- brown particles of SnS_2 powder were obtained and were ground into a fine powder using a mortar- pestle[20].

2.3 Synthesis of $SnSe_2$ Powder

Tin (IV) chloride penta-hydrate (1.5 mmol) was mixed into 30 mL of de-ionized water and was labeled as solution 'A'. Selenium dioxide (1.5 mmol) was added into 10 mL of di-water and was labeled as solution 'B'. Both 'A' and 'B' were mixed and stirred for 20 minutes. Then 3 mL of hydrazine-hydrate was added into the solution and it was magnetically stirred for 20 minutes at room temperature. It was then transferred into a teflon container and sealed into a stainlesssteel autoclave. The solution was then heated in the hot air oven at 200 °C for 24 hours. Post this, the sample was washed twice with de-ionized water and ethanol and centrifuged for 6 minutes at 5500 rpm. It was then left to dry in a vacuum oven overnight at 80 °C. Black particles of $SnSe_2$ were obtained and were grinded into a fine powder using a mortar- pestle[40]. for 15 minutes[41].

2.4 Synthesis of $SnS_2/SnSe_2$ Heterostructure Powder

Tin (IV) chloride penta-hydrate (5 mmol) and Selenium dioxide (1 mmol) were taken and mixed into 40 mL of ethylene glycol solution. The solution was magnetically stirred for 45 minutes. After which 3 mL of Hydrazine hydrate was added into it drop-by-drop in the form of a reducing agent to reduce SeO_2 present in the precursor solution to Se species. Apart from this, it also assisted in the controlled nucleation and interfacial growth between SnS_2 and $SnSe_2$ for heterostructure formation. This was followed by the addition of already prepared SnS_2 powder into the solution for physical mixing. The solution was then stirred for 30 minutes at 70 °C. The solution was then kept in the hot air oven at 200 °C for 24 hours. Post this, the sample was washed thrice with deionized water and ethanol and centrifuged for 10 minutes at 5500 rpm. It was then left to dry in a vacuum oven for 12 hours at 80 °C. The powder obtained was black in colour and was grinded using a mortar- pestle for 15 minutes[41].

2.5 Synthesis Methodology of TMDCs/PVDF Films

The synthesized powders were then integrated with a flexible and piezoelectric polymer PVDF to synthesize composite films. For the synthesis of films, 1g PVDF was mixed in 10 mL DMF and was magnetically stirred for 3 hours. The synthesized powders were mixed into the PVDF solution at varying weight percentages of 1, 3, 5 and 7 wt % corresponding to 10 mg, 30 mg, 50 mg and 70 mg nanofiller content, respectively and stirred for 2 more hours. Post which, the solution was ultra-sonicated for 30 minutes and was stirred again for 30 minutes. Then the final prepared mixture was casted on glass slides using a pipette and was left for drying in the oven at 60 °C for 12-15 hours in Fig. 1. Finally, the films were retrieved from the oven and cleaned with DI water and stored in vacuum[39].

2.6 Fabrication of PENG

For device fabrication, the synthesized films were cut down in rectangular shape to their requisite size of

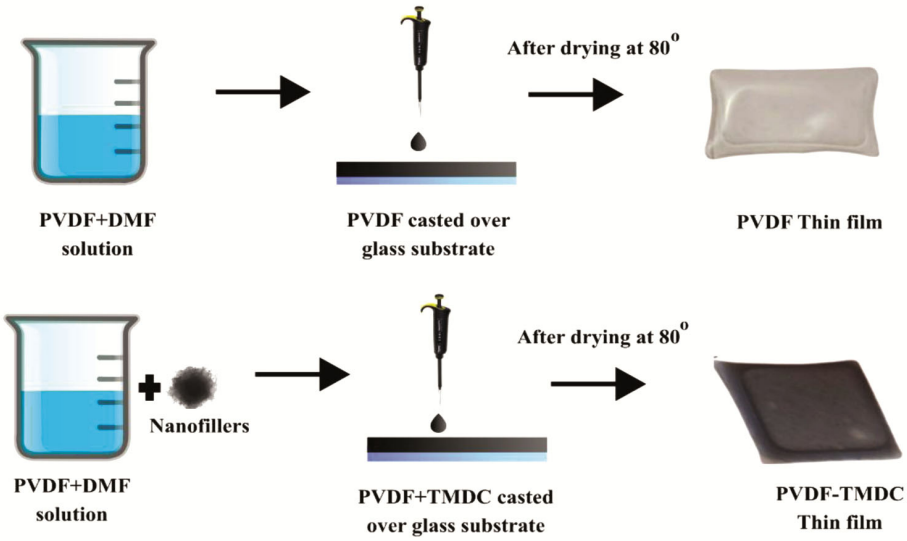

Fig. 1 — Schematic representation of the fabrication route for PVDF/TMDC composite thin films

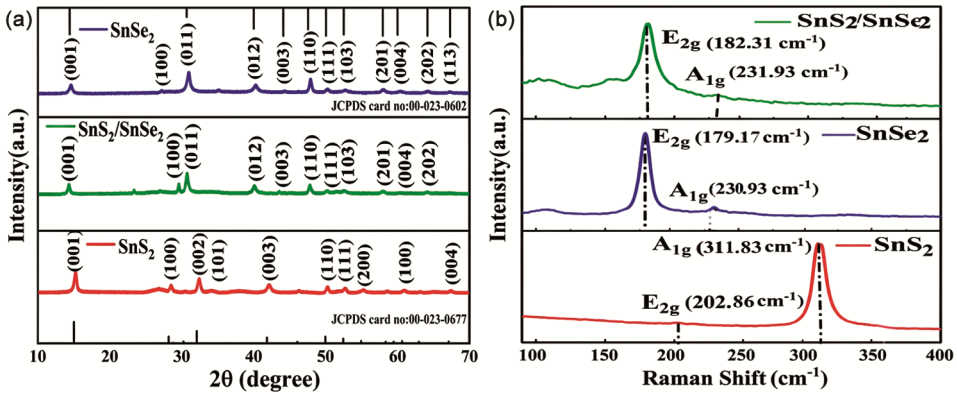

Fig. 2 — (a) X-ray diffraction (XRD) results; and (b) Raman spectra of synthesized SnS_2, $SnSe_2$ and $SnS_2/SnSe_2$ heterostructure powders

2x3 cm^2. These films were then embedded between aluminium adhesive tapes, thus forming the electrodes for the PENG devices. Following this, the aluminium electrodes from both sides were attached to thin Copper tape strips and were soldered to form a connection between the PENG and the digital measurement device. The formed PENG devices were then encapsulated by kapton tape.

3 Characterization Techniques

XRD was done using the X-ray diffractometer Cu X-ray source, 3 kW Bruker D8 discoverer for synthesized powder samples in which the peaks confirmed the correct formation of the powder[42]. FTIR spectra were recorded in order to check the content of the electro active , β- phase using the Perkin Elmer Spectrum II device. This confirmed the crystallization of electro active β-phase in the synthesized films. Raman spectroscopy was done employing the Horiba Jobin-Yvon LABRAM-HR spectrometer in order to check the vibrational phases of the material. FESEM revaled the morphology of the films' surface and microstructural information. The PE loop analysis of the films was obtained using a PE loop tracer. The open-circuit voltage (peak-to-peak) (V_{oc}) and short-circuit current (I_{sc}) measurements were done to check the open loop current and voltage values of fabricated devices using the digital storage oscilloscope (Tektronix, MD034) and a electrometer (Keithly DMM6517B).

4 Results and Discussion

XRD analysis as shown in the Fig. 2 (a) was used to analyse the structural and crystalline properties of SnS_2, $SnSe_2$ and $SnS_2/SnSe_2$ heterostructure. For SnS_2, the peaks were observed at 15.20°, 28.55°, 32.29°, 42.12°, 50.24°, 52.66°, 55.22°, 60.95°and 67.43° at corresponding planes (001), (100), (002), (003),

(110), (111), (200), (100) and (004) respectively in accordance to JCPDS card no. 00-023-0677. For $SnSe_2$, the peaks were noticed at 14.59°, 30.95°, 40.31°, 47.91°, 50.28°, 52.76°, 57.99°, 60.53°, 64.17° and 67.31° at corresponding planes (001), (011), (012), (110), (111), (103), (201), (004), (202) and (113) respectively in agreement with the standard diffraction pattern as per the JCPDS card no. 00-023-0602. XRD indicates the coexistence of SnS_2 and $SnSe_2$ phases in the heterostructure. The peaks for the heterostructure were observed at 14.26°, 26.98°, 29.50°, 30.75°, 40.12°, 43.47°, 47.81°, 50.18°, 52.70°, 58.01°, 60.52° corresponding to the planes (001), (100), (011), (012), (003), (110), (111), (201), (004) respectively. Out of which, the diffraction peaks at 14.26°, 29.50°, 43.47°, 50.18°, and 52.70° correspond to SnS_2. Similarly, the peaks at 26.98°, 30.75°, 40.12°, 47.89°, 58.01°, 60.52° and 64.02° correspond to $SnSe_2$.

Figure 2 (b) depicts Raman spectra of the powders along with two Raman active peaks namely E^1_{2g} and A_{1g}. The A_{1g} mode represents the out-of-plane vibrations of the S atoms while the E^1_{2g} mode corresponds to the in-plane and anti-phase vibrations of S atoms relative to Sn[43]. Their peaks were recorded at 202.86 cm^{-1} and 311.83 cm^{-1} respectively for SnS_2. For $SnSe_2$, the peaks were seen at 179.17 cm^{-1} and 230.93 cm^{-1}. The observed peaks for heterostructure were at 182.31 cm^{-1} and 231.93 cm^{-1}. In our composite nanostructure, the major Raman peaks do not overlap with individual characteristic peaks of SnS_2 along with $SnSe_2$, thus confirming that a uniformly distributed nanostructure was synthesized successfully.

The XRD for flexible films is shown in Fig. 3 (a), which confirms the effective incorporation of 2D nanofillers into the PVDF polymer matrix. For the α-phase, the peak is detected at 18.4° and for the polar β-phase it is detected at 20.2°. The XRD results represent the peaks corresponding to PVDF, SnS_2 and $SnSe_2$ by ✱, # and $ respectively. This data shows the co-existence of TMDC materials and the β phase in synthesized composite films. Presence of crystalline polar β-phase in bare PVDF is also observed.

To analyse the polar crystalline phases and the phase transformation of PVDF/TMDC films at 3 wt %, FTIR spectroscopy was performed. In Fig. 3 (b), the β-phase is evaluated from the vibrational band seen at 840 cm^{-1} and α-phase at 762 cm^{-1}. These bands map to the unique bending and stretching modes occurrence of β- as per the polar crystalline phases of PVDF. The peaks seen at 840 cm^{-1}, 1279 cm^{-1} and 1400 cm^{-1} show the phase, defined as inherently piezoelectric. It is inferred that by the inclusion of TMDC materials, the β-phase of bare PVDF gets enhanced which is shown in Table 1. By using the Beer- Lambert law, , β- phase was calculated as per Eq. (1)[44].

$$F(\beta) = \frac{A_\beta}{\left(\frac{K_\beta}{K_\alpha}\right)A_\alpha + A_\beta} \quad \ldots (1)$$

where, K (β) = 7.7x10^4 cm^2/mol and K (α) = 6.1x10^4 cm^2/mol, are coefficients corresponding to the absorption at 840 cm^{-1} and 762 cm^{-1}. The β phase was evaluated to be 61 % for bare PVDF and after adding 3 wt % of TMDC nanofillers within the PVDF matrix, the β phase was calculated to be 72 %, 70 % and 76 % respectively. The β phase for different materials was calculated which is shown in Table 1. Since PVDF/SnS_2/$SnSe_2$ films exhibited the maximum value of electro-active β phase, its films at varying weight percentages (1 %, 3 %, 5 % and 7 %) were prepared and the highest value was observed at 3 wt %.

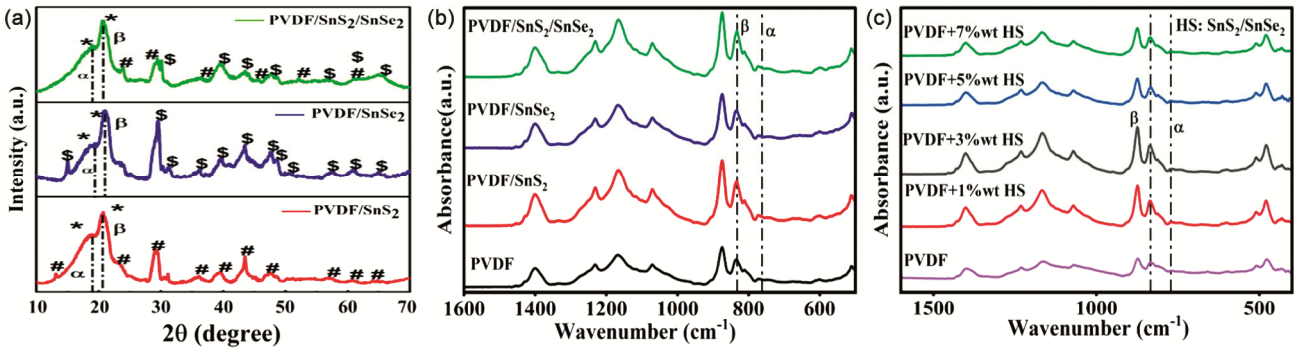

Fig. 3 — (a) XRD (b) FTIR spectra of PVDF composites with different TMDC nanofillers at 3 wt %; and (c) FTIR spectra of PVDF based composites with varying SnS_2/$SnSe_2$ heterostructure nanofiller concentration

Table 1 — Comparative analysis of β phase for different nanofiller at 3 wt %. in the PVDF matrix

Material	Electro active β phase (%)
Bare PVDF	61
PVDF/SnS_2	72
PVDF/$SnSe_2$	70
PVDF/SnS_2/$SnSe_2$	76

Table 2 — Comparison of β-phase as a function of $SnS_2/SnSe_2$ heterostructure nanofiller concentration

Wt. % of $SnS_2/SnSe_2$	β-phase (%)
0	61
1	77.8
3	81.5
5	76.2
7	75.6

As the weight percentage of the heterostructure nanofiller was increased, an enhancement in the β-phase content was observed, thus indicating its effective role in promoting electroactive β-phase formation. The β-phase fraction reached a maximum value at 3 wt %, suggesting an optimal filler concentration for nucleation and the stability of phase. Beyond this concentration, it was observed that the β-phase content had declined, which could be attributed to nanofiller agglomeration. This trend is clearly summarized in Table 2 and shown graphically through Fig. 3 (c).

To analyse the morphology of the PVDF/TMDC films, FESEM was performed. In the FESEM images of films, as shown in Fig. 4 (a-d), it is visible that the distribution of SnS_2, $SnSe_2$ and SnS_2 /$SnSe_2$ in PVDF polymer matrix is uniform without any agglomeration, which implies effective arrangement of nanofillers inside the PVDF polymer matrix.

PE hysteresis study of thin films was also done to compute the piezoelectric retentivity and to elaborate on the intrinsic dipole behaviour which is directly linked to their piezoelectric performance which is shown in the Fig. 4 (e). This comparative study of hysteresis loop shows the presence of polarization switching under the influence of an applied electric field, hence confirming the presence of the non centro-symmetric polarization domains in these PVDF enhanced layered dichalcogenide systems. The heterostructure shows an enhanced value of remnant polarization (P_r) as compared to pristine SnS_2 and $SnSe_2$. Hence the $SnS_2/SnSe_2$ heterostructure exhibits an improved value of remnant polarization implying substantial dipole alignment and charge redistribution across the physically created interface. The remanent polarization (P_r) values for PVDF,

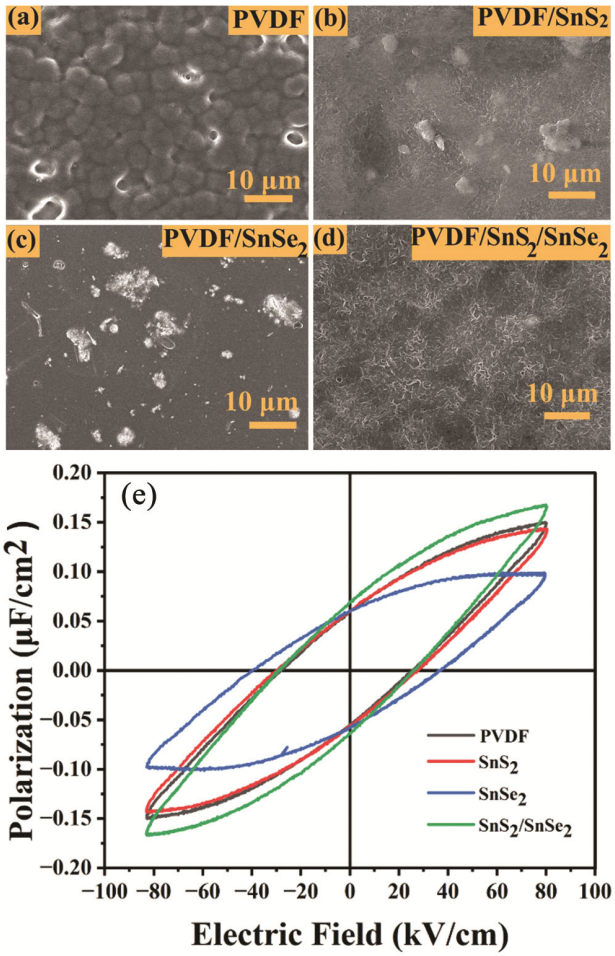

Fig. 4 — FESEM micrographs for (a) PVDF (b) PVDF/ SnS_2 (c) PVDF/$SnSe_2$ (d) PVDF/SnS_2/$SnSe_2$, and (e) PE loop for PVDF, PVDF/SnS_2, PVDF/$SnSe_2$ PVDF/SnS_2/$SnSe_2$ thin films

PVDF/SnS_2, PVDF/$SnSe_2$, PVDF/SnS_2/$SnSe_2$ were calculated and found to be 6.13 × 10^{-2} μF cm^{-2}, 7.49× 10^{-2}μF cm^{-2}, 7.58× 10^{-2}μF cm^{-2} and 8.78× 10^{-2} μF cm^{-2} respectively. This enhanced behaviour of remnant polarization is directly linked with the generation of a stronger piezoelectric potential under mechanical perturbation which leads to efficient charge separation and migration. Hence, the enlarged hysteresis loop observed for the heterostructure can be linked to the improved polarization and hence confirms their superior piezoelectric efficiency.

For assessing the piezoelectric performance of fabricated PVDF films incorporated with 3 wt.% of each of the 2D nanofillers (SnS_2, $SnSe_2$ and $SnS_2/SnSe_2$), the open-circuit voltage (peak-to-peak) (V_{oc}) and short-circuit current (I_{sc}) was determined as depicted in Figs. 5 and 6. These measurements were

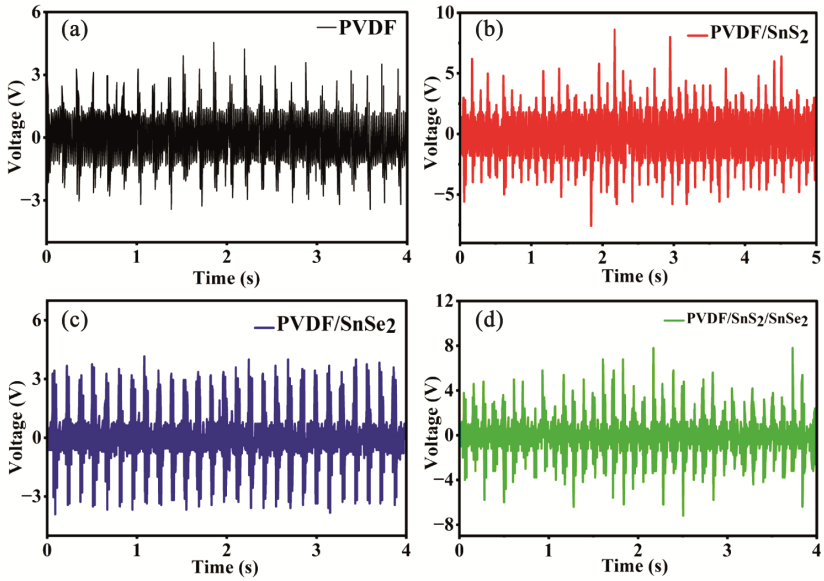

Fig. 5 — Open circuit voltage (peak-to-peak) of (a) PVDF (b) PVDF/SnS_2 (c) PVDF/$SnSe_2$; and (d) PVDF/SnS_2/$SnSe_2$ nanogenerators for a tapping frequency of 7Hz

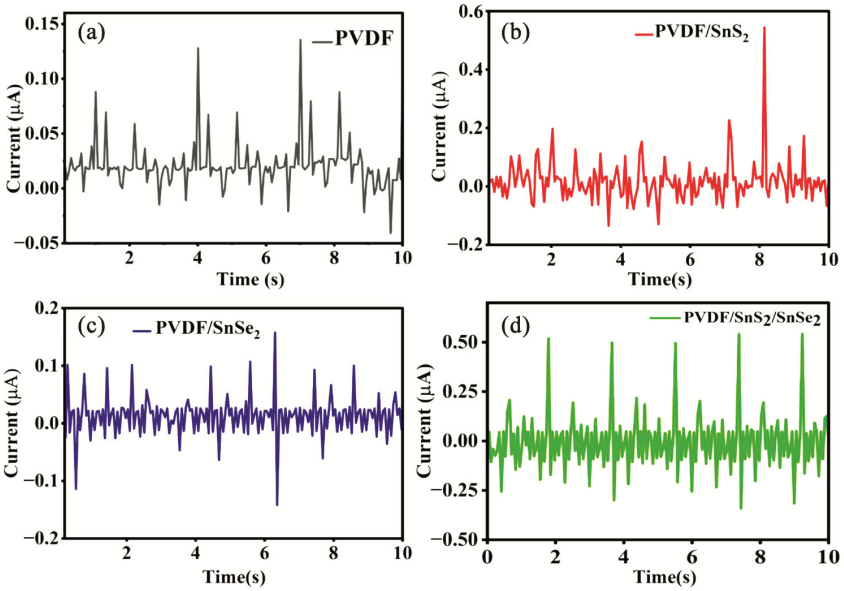

Fig. 6 — Short circuit current of (a) PVDF (b) PVDF/SnS_2 (c) PVDF/$SnSe_2$, and (d) PVDF/SnS_2/$SnSe_2$ nanogenerators for a tapping frequency of 7 Hz

made using an oscilloscope (Tektronix MD034) and an electrometer (Keithly 6517B). These values directly indicate the induced piezoelectric voltage, thereby signifying the efficient piezoelectric results of the samples. A higher value of V_{oc} and I_{sc} exhibits better charge separation and effective dipole alignment. The maximum response for the films was observed at a frequency of 7 Hz. The experimental value for V_{oc} was observed to be 5.8 V for bare PVDF, however when incorporated with TMDC nanofillers, the resultant voltage was enhanced to be 10.8 V, 7.4 V and 13.2 V for SnS_2, $SnSe_2$, and SnS_2/$SnSe_2$ respectively. Following the similar trend, the short-circuit current of the fabricated piezoelectric devices was reported as 0.15 μA, 0.57 μA, 0.29 μA and 0.87 μA corresponding to bare PVDF, PVDF/SnS_2, PVDF/$SnSe_2$ and PVDF/SnS_2/$SnSe_2$. All these values of $V_{oc,}$ I_{sc} and P_r are compiled in Table 3. This enhancement in the values of V_{oc} and I_{sc} corresponds to the combined effects of enhanced

β phase nucleation and intrinsic piezoelectricity of 2D nanofillers[32]. Further enhancement in the piezoelectric response for $SnS_2/SnSe_2$ based PVDF film is due to inbuilt electric field and interfacial dipoles which facilitates charge separation and enhanced carrier transport across the interface[26]. Therefore, the heterostructure stands out as the most promising candidate for energy harvesting applications.

To show the superior performance of the fabricated PENG device in this study, its piezoelectric response is compared with other similar reported studies on 2D materials as shown in Table 4. It clearly shows that the piezoelectric response of the PENG based on $PVDF/SnS_2/SnSe_2$ heterostructure is better than the other reported devices.

Table 3 — Comparison of piezoelectric output of PVDF and TMDC nanocomposite films

Nanogenerator	V_{oc} (V)		
PVDF	5.8	0.15	6.13×10^{-2}
$PVDF/SnS_2$	10.8	0.57	7.49×10^{-2}
$PVDF/SnSe_2$	7.4	0.29	7.58×10^{-2}
$PVDF/SnS_2/SnSe_2$	13.2	0.87	8.78×10^{-2}

5 Piezoelectric Nanogenerator (PENG)

Our present work reports the fabrication of flexible piezoelectric nanogenerators using PVDF enhanced Tin based 2D dichalcogenides namely SnS_2, $SnSe_2$ and their heterostructure $SnS_2/SnSe_2$. A PENG works on the principle of piezoelectric effect, converting any form of mechanical stress and deformities into electrical energy. In its initial state as shown in Fig. 7, that without any applied force, the dipoles inside the PVDF based matrix are randomly oriented creating no net electrical output. When a periodic mechanical stress is applied, the film undergoes deformation, causing an alignment within dipoles, thereby generating a piezoelectric potential across the electrodes. This causes an accumulation of charge on the electrodes producing a potential difference which causes electrons to move through the external circuitry. Upon releasing the applied force, the dipoles revert back to their original state, hence creating a reversed charge flow. This periodic process of deformation and relaxation induces alternating electrical signals corresponding to successive cycles of compression and release.

Table 4 — Performance Comparison of piezoelectric output TMDC–PVDF Nanogenerators

Device configuration	Voltage generated	Current generated	Synthesis method	References
PVDF/KNN-ZS nanofibrous web[45]	1.68 V	0.216 μA	Electro spinning	[45]
$PVDF/MoS_2$ quantum sheets[46]	0.9 V	25 μA	Solution casting	[46]
PVDF-rGO-MoS_2[47]	2.4 V	0.68 μA	Solution casting	[47]
$PVDF/MoS_2$ @ZnO[48]	6.2 V	528 nA	Solution Casting	[48]
PVDF-MoS_2[39]	9.8 V	0.9 μA	Drop-casting	[39]
$PVDF/SnS_2/SnSe_2$	13.2V	0.87 μA	Drop-casting	Present work

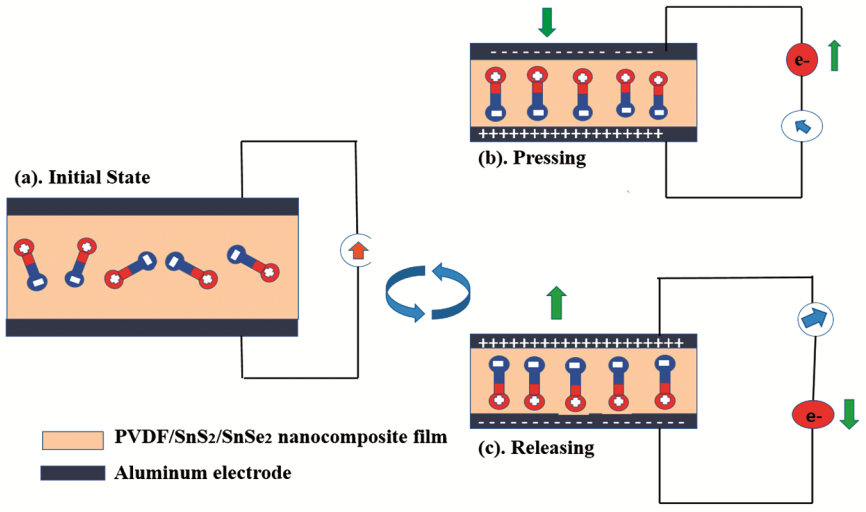

Fig. 7 — Schematic of piezoelectric response of $PVDF/SnS_2/SnSe_2$ based device with aluminium electrodes: (a) initial dipole orientation (b) dipole alignment under pressing; and (c) reversed electron flow upon releasing

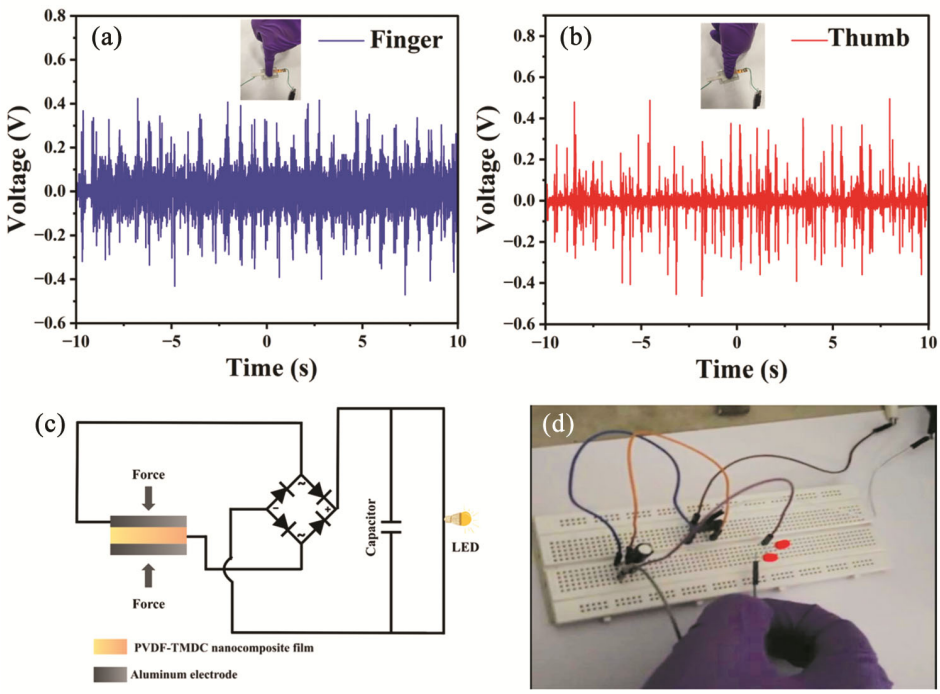

Fig. 8 — Open-circuit voltage (peak-to-peak) of PENG under applied force from (a) finger (b) thumb (c) Schematic illustration of PENG circuit for operating an LED; and (d) LED powered by PENG

For evaluating the electrical response of the devices, the $SnS_2/SnSe_2$ heterostructure based PENG was exposed to periodic mechanical stress. When subjected to biomechanical stimuli, using single finger and thumb tapping, the device exhibited an output voltage of 0.67 V and 0.74 V respectively, as shown in Fig. 8 (a) and (b). The resulting alternating piezoelectric response was made to pass through a bridge rectifier circuit to convert it into a unidirectional signal as shown in Fig. 8 (c). Post this, the rectified output was stored in a capacitor thus enabling effective charge accumulation and stable energy delivery to the external loads. The obtained output was thus rectified and stored in the capacitor and was successfully used to power an LED shown in Fig. 8 (d).

The open circuit voltage (peak-to-peak) and short circuit current values exhibited a stable and periodic signal over multiple cycles, thereby indicating that the nanocomposite films are mechanically robust and possess good durability. Among all the devices, the heterostructure based PENG demonstrated a superior electrical output. In addition to this, the presence of SnS_2 and $SnSe_2$ with distinct chalcogen atoms further enhances the asymmetric charge distribution and efficient charge separation within the nanofiller induced PVDF matrix.

This improved electrical output was supported by the XRD and FTIR analysis which confirmed the enhanced dipole alignment along with the effective incorporation of nanofillers within the PVDF polymer matrix. All these results showed the potential of Tin based dichalcogenides heterostructure integrated with PVDF for its application in flexible, self-powered and wearable energy harvesting systems.

6 Conclusion

This work successfully shows the fabrication of PVDF/SnS_2, PVDF/$SnSe_2$ and PVDF/SnS_2/$SnSe_2$ heterostructure films. SnS_2, $SnSe_2$ and their heterostructure were synthesized using the hydrothermal route, then the obtained powders were used as nanofillers within the PVDF polymer matrix. Further, PVDF-based composite thin films were fabricated using the drop-casting technique. The $SnS_2/SnSe_2$ heterostructure integrated PENG demonstrated the maximum output performance. The remanent polarization of PVDF, PVDF/SnS_2, PVDF/$SnSe_2$, PVDF/SnS_2/$SnSe_2$ was evaluated from the PE loop and was reported to be 6.13×10^{-2} μF cm^{-2}, 7.49×10^{-2} μF cm^{-2}, 7.58×10^{-2} μF cm^{-2} and 8.78×10^{-2} μF cm^{-2} respectively. The open-circuit voltage (peak-to-peak) was observed as 5.8 V, 10.8 V,

7.4 V and 13.2 V for bare PVDF, PVDF/SnS_2, PVDF/$SnSe_2$, and PVDF/SnS_2/$SnSe_2$ respectively. The short-circuit current was reported as 0.15 μA, 0.57 μA, 0.29 μA and 0.87 μA corresponding to bare PVDF, PVDF/SnS_2, PVDF/$SnSe_2$ and PVDF/SnS_2/$SnSe_2$. The fundamental reasons responsible for this enhanced performance of heterostructure based PENG device is the improved value of electroactive β-phase, and the superior values of remnant polarization within the PVDF films post the incorporation of TMDC nanofillers. The device was evaluated under biomechanical stimuli, including single finger and thumb tapping to demonstrate the practical applicability of the fabricated devices. On combining all the above obtained results, the PENG integrated with heterostructure SnS_2/$SnSe_2$ exhibited the most superior performance. Therefore, we propose that this device could be effectively utilized for harnessing electrical energy from mechanical energy and for driving the operation of low powered electronic systems and devices. Our design successfully demonstrates an efficient, scalable and robust PENG with a high capability of converting mechanical energy into electrical energy.

Acknowledgement

The authors expresses gratitude to the Government of India's SERB-SURE project (project no. SUR/2022/005243) and Delhi Technological University for their financial support. The author Pragya Dobhal acknowledges the financial assistance received through the DST INSPIRE Scholarship awarded by the Department of Science and Technology, Government of India (IVR No. 202100014550).

References

1 Tang C W & VanSlyke S A, *Appl Phys Lett*, 51 (1987) 913.
2 Jang H J, Lee J Y, Kwak J, Lee D, Park J H, Lee B & Noh Y Y, *J Inform Disp*, 20 (2019) 1.
3 Choi S, Kang C, Byun C W, Cho H, Kwon B H, Han J H, Yang J H, Shin J W, Hwang C S, Cho N S, Lee K M, Kim H O, Kim E, Yoo S & Lee H, *Nat Commun*, 11 (2020) 2732.
4 Vijayakanth T, Shankar S, Finkelstein Zuta G, Rencus Lazar S, Gilead S & Gazit E, *Chem Soc Rev*, 52 (2023) 6191.
5 Mohammadpourfazeli S, Arash S, Ansari A, Yang S, Mallick K & Bagherzadeh R, *RSC Adv*, 13 (2023) 370.
6 Ahbab N, Naz S, Xu T B & Zhang S, *Micromachines*, 16 (2025) 386.
7 Rui G, Allahyarov E, Zhu Z, Huang Y, Wongwirat T, Zou Q, Taylor P L & Zhu L, *Responsive Mater*, 2 (2024) e20240002.
8 Zhao T, Li Y & Zhang Z, *Chem Commun*, 62 (2026) 3406.
9 Upadhye P A, Roy Chowdhury S, Kumar V, Ranjan R, Kumar S, Mondal S, Oh J & Misra M, *Sci Rep*, 15 (2025) 19885.
10 Kushwaha A, Peter A T, Shah F U & Gupta D, *Mater Adv*, 7 (2026) 813.
11 Mankuni A & Varghese S, *Nano Energy*, 140 (2025) 111042.
12 Adaval A, Bhatt B B, Singh S, Gupta D, Maji P K, Aslam M, Turney T W, Simon G P & Bhattacharyya A R, *J Phys Chem C*, 127 (2023) 6483.
13 Raza A, Hassan J Z, Ikram M, Ali S, Farooq U, Khan Q & Maqbool M, *Adv Mater Interfaces*, 8 (2021) 2002205.
14 Chatterjee A, Das A, Saha K & Jeong U, *Adv Sensor Res*, 2 (2023) 2200080.
15 Pang F, Zhao P, Lee H Y, Kim D J, Meng X, Cho Y S & Kim S W, *Adv Sci*, 12 (2025) 2411422.
16 Zi Y, Zhu J, Hu L, Wang M & Huang W, *Small Sci*, 2 (2022) 2100098.
17 Tannarana M, *Eur Phys J Plus*, 139 (2024) 843.
18 Peiris B, *Adv 2D Mater Beyond Graphene*, (2025), http://dx.doi.org/10.2139/ssrn.5602072.
19 Muduli S P, Veeralingam S, Das N K & Badhulika S, *Mater Res Bull*, 178 (2024) 112923.
20 Junaidu M H, Liew J Y C, Onimisi M Y, Tafida R A, Bello M, Adezuka Y, Owolabi J A & Lawal H A, *J Mater Sci Mater Electron*, 35 (2024) 380.
21 Maity S, Kar E & Sen S, *ACS Appl Mater Interfaces*, 16 (2024) 68294.
22 Chen Z, Zhang W, Qu X & Zhang Y, *Theranostics*, 16 (2026) 3136.
23 Liu Y, Huang Y & Duan X, *Nature*, 567 (2019) 323.
24 Lu C, Zhang S, Chen M, Chen H, Zhu M, Zhang Z, He J, Zhang L & Yuan X, *Front Phys*, 19 (2024) 53206.
25 Gupta N, Sachin S, Kumari P, Rani S & Ray S J, *RSC Adv*, 14 (2024) 2878.
26 Yang C, Zhang X, Li Y, Wang J, Liu H & Zhao Q, *Appl Surf Sci*, 710 (2025) 163836.
27 Sekar U, Radhakrishnan J & Biswas K, *Sustain Energy Fuels*, 9 (2025) 5399.
28 Xing R, Li H, Wang Y, Zhang Q, Chen Z & Liu J, *Adv Mater*, 37 (2025) 2501833.
29 Cao V A, Li Q, Nguyen T H, Chen Y, Huang X & Wang Z L, *ACS Nano*, 15 (2021) 10428.
30 Xiao Y, Zhang J, Liu X, Chen H, Li Y, Wang P, Zhao L & Xu H, *Chem Soc Rev*, 52 (2023) 1215.
31 Cong X, Shah M N U & He W, *J Mater Chem C*, 12 (2024) 5411.
32 Singh V, Meena D, Sharma H, Trivedi A & Singh B, *Energy*, 239 (2022) 122125.
33 Kim G, Yun J & Kim D, *Nano Energy*, 126 (2024) 109678.
34 Mohebbi E, Pavoni E, Pierantoni L, Stipa P, Laudadio E & Mencarelli D, *J Phys Chem Solids*, 185 (2024) 111755.
35 Wen L, Cheng F, Zhao X, Han L, Zhao D & Wang S, Nanomaterials, 15 (2025) 850.
36 He Q & Briscoe J, *ACS Appl Mater Interfaces*, 16 (2024) 29491.
37 Kou L, Haque R, Sadri R, Auliya R Z, Kaur M, Roberts E P L, Gan W C, Haniff M A S M, Dee C F & Ooi P C, *Ind Eng Chem Res*, 63 (2024) 15853.
38 Yempally S, Bhapkar A R, Prasad R, Laad M, Bhame S & Ponnamma D, *Discover Polymers*, 2 (2025) 7.

39 Singh V & Singh B, *J Alloys Compd*, 941 (2023) 168850.
40 Wen L, Cheng F, Zhao X, Han L, Zhao D & Wang S, *Nanomater*, 15 (2025) 850.
41 Liu L, Song D, Kaiser M E, Liu J, De Yoreo J J & Sushko M L, *Small*, 21 (2025) 2410526.
42 Panda S, Antonakos A, Liarokapis E, Bhattacharya S & Chaudhuri S, *Mater Res Bull*, 42 (2007) 576.
43 Borisenko D, Kargin N & Rybin M, *J Appl Spectrosc*, 92 (2025) 762.
44 Cai X, Lei T, Sun D & Lin L, *RSC Adv*, 7 (2017) 15382.
45 Banerjee S, Bairagi S & Ali S W, *Energy*, 244 (2022) 123102.
46 Nardekar S S, Krishnamoorthy K, Pazhamalai P, Sahoo S & Kim S J, *Nano Energy*, 93 (2022) 106869.
47 Faraz M, Singh H H & Khare N, *J Alloys Compd*, 890 (2022) 161840.
48 Cao S, Zou H, Jiang B, Li M & Yuan Q, *Nano Energy*, 102 (2022) 107635.